Drift gas optimization for cylindrical geometries with application to the largest detector to date

by

Jesse J. Kirchner

Submitted to the Department of Physics
in partial fulfillment of the requirements for the degree of

Bachelor of Science in Physics

at the

MASSACHUSETTS INSTITUTE OF TECHNOLOGY

June 2000

Author ....
Department of Physics
May 5, 2000

Certified by ....
Ulrich J. Becker
Professor of Physics
Thesis Supervisor

Accepted by ....
David E. Pritchard
Thesis Coordinator

Drift gas optimization for cylindrical geometries with application to the largest detector to date

by

Jesse J. Kirchner

Submitted to the Department of Physics
on May 5, 2000, in partial fulfillment of the
requirements for the degree of
Bachelor of Science in Physics

Abstract

Drift tubes in magnetic fields are widely used for particle path reconstruction in huge new detectors such as ATLAS at LHC, CERN. Complete understanding of the drift features of electrons in the proposed gas mixture is needed to optimize detector resolution. This can be accomplished by determining a drift gas with linear space-time characteristics despite the problem of an $E \propto \frac{1}{r}$ drift field. Electron mean drift velocity and magnetic deflection angle were measured in various gas mixtures at a pressure of 3 bar over a range of electric and magnetic fields. ATLAS chose high pressures to limit inaccuracy caused by diffusion. Comparison of velocity and angle data at different magnetic fields yields scaling laws for magnetic field effects. Accurate measurements at 3 bar and 1 bar show E/P and B/P scaling, allowing predictions of drift behavior at intermediate pressures. The space-time response is predicted by adapting the data to a cylindrical geometry. ATLAS MDT results were reproduced for the original design mixture Ar:CH_4:N_2 (91:5:4)% and the default mixture Ar:CO_2 (93:7)% which will not reach design accuracy. By comparison, several other mixtures with better space-time linearity were determined. Two mixtures of Ar:N_2:CO_2 at percentages of (92:6:2) and (94:2:4) showed increased reconstruction accuracy.

Thesis Supervisor: Ulrich J. Becker
Title: Professor of Physics

Acknowledgments

The author would like to acknowledge: Prof Ulrich Becker and Prof Peter Fisher at MIT for guidance, Evan Fortunato and Catherine Reyes for editing, Prof Steven Ahlen at Boston University for MDT chamber pictures, Adrian Fabich, Chris Fabjan, and Emma Rieder for tours of the ATLAS facilities at CERN, Michael Grossman and Fred Coté for technical advice and machining help, Rafael Dinner for hardware and software development, Reyco Henning for magnet calibration, and Krzysztof Fidkowski, Karlene Rosera, Jesse Wodin, Julie Wyatt, and Alyssa Bishop for support.

Contents

List of Figures

Chapter 1

Introduction

Accurate reconstruction of particle paths is necessary for measurements of particle momenta and scattering angles. In gaseous detectors this requires an understanding of electron drift properties such as drift velocity and magnetic deflection angle in different gas mixtures. Measurement of these quantities over a range of electric and magnetic fields enables designers of gaseous detectors to make informed decisions regarding design.

The use of an optimized drift gas will be discussed in terms of the ATLAS[1] Monitored Drift Tube (MDT) system, which uses 370 000 drift tubes in 1 194 chambers (Fig. 1-2) with an expected space resolution of 80 μm [1]. While the originally proposed gas mixture Ar:CH_4:N_2 (91:5:4)% met this resolution requirement, it was found that mixtures with hydrocarbon admixtures such as CH_4 are prone to ageing [2] [3] [4]. The mixture Ar:CO_2 (93:7)% was subsequently used because of its resistance to ageing.

The ATLAS MDT drift gas will be kept at a pressure of 3 bar to reduce diffusion and ionization fluctuation [1]. In order to understand the effects of pressure variations on mean drift velocity and magnetic deflection angle, data at 1 and 3 bar were measured and compared. Also, a method of scaling for different magnetic fields is presented, simplifying both data correction in non-homogeneous fields and communi-

[1]A Toroidal LHC ApparatuS (Fig. 1-1).

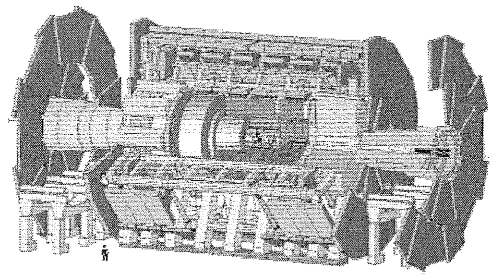

Figure 1-1: Schematic representation of the ATLAS detector [5].

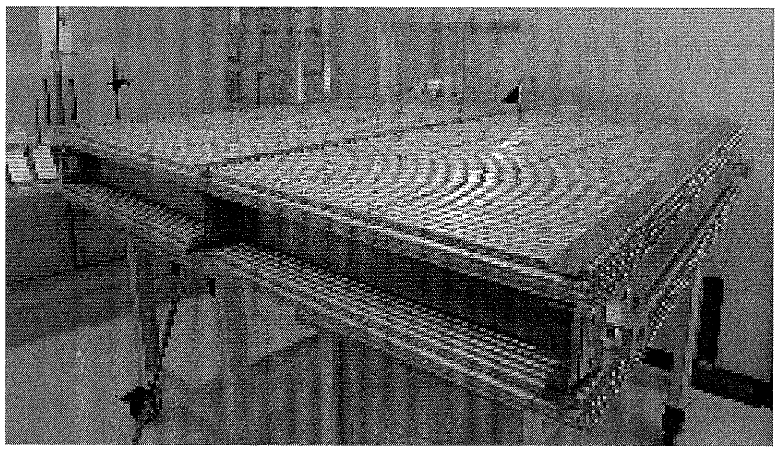

Figure 1-2: MDT chamber used for testing in the Boston Muon Consortium chamber construction clean room at the Harvard High Energy Physics Lab [6].

cation of experimental results.

Detectors employing drift tubes in magnetic fields must be able to accurately reconstruct particle paths in these cylindrical geometries. While better position resolution cannot come from the magnets, which are at the limit of superconducting technology, better position resolution can be reached by choosing an appropriate drift gas and understanding it well.

To achieve high accuracy in coordinate reconstruction, it is important to keep corrections small. This means having a linear space-time relation, meaning that the electron mean drift velocity is nearly independent of electric field. Also, in large systems operating for long periods of time, the drift gas must have high tolerance for cumulative contamination by H_2O and N_2 from air, however O_2 is usually removed by purifiers. Surprisingly, the effects of small amounts of N_2 are significant [7], but can be used advantageously by using N_2 as an admixture in the gas mixture [8].

As seen in Fig. 1-3, the space-time relation for the original ATLAS mixture $Ar:CH_4:N_2$ (91:5:4)% is very linear unlike the relation for the current mixture $Ar:CO_2$ (93:7)%.

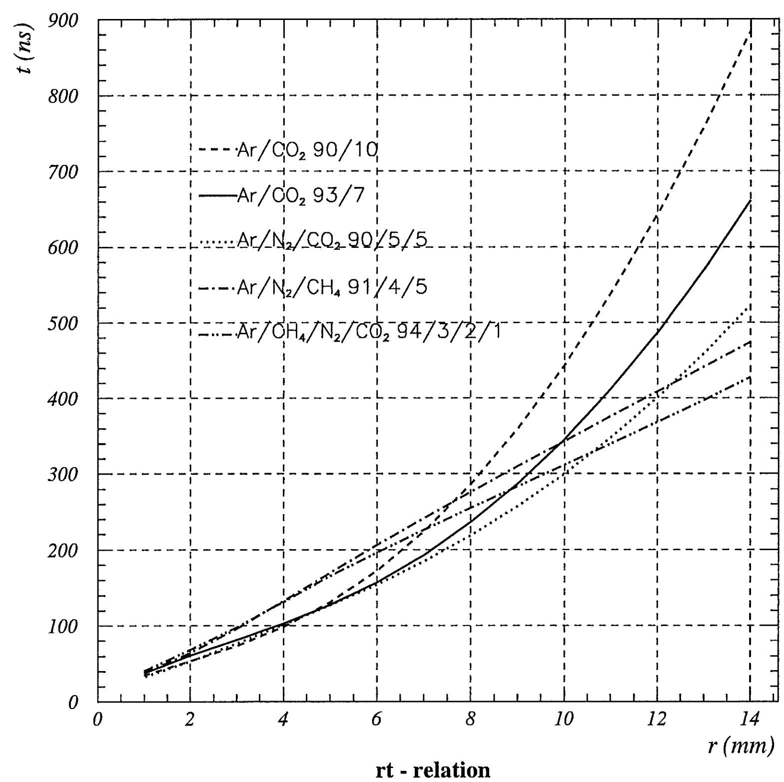

Figure 1-3: Space-time relations for different gas mixtures [4]. The original design gas was $Ar:CH_4:N_2$ (91:5:4)% and the present operational gas is $Ar:CO_2$ (93:7)%.

Knowledge of properties of electron drift in gaseous detectors will allow for a systematic search for a gas mixture which improves upon the currently used mixture and improves coordinate accuracy. To avoid ageing, it is important to find a mixture with a linear space-time relation which does not include a hydrocarbon admixture.

Chapter 2

Theory

In order to optimize the operation of gaseous particle detectors, the ionization and behavior of electrons moving in a gas and in electric and magnetic fields must be known. Electron-ion pairs are created by ionization when a high energy particle deposits energy in the gas. The energy loss $\frac{dE}{dx}$ is described by the Bethe-Bloch Formula [9]. For a high energy muon ($10^2 < \gamma < 10^3$) in pure argon gas at 3 bar, the average $\frac{dE}{dx}$ is about 14 keV/cm. The average amount of work required to ionize an argon atom is 26.4 eV [10], yielding an average of 540 primary electrons per cm. After the electrons come to thermal equilibrium, the distribution of velocities can be derived from the Maxwell-Boltzmann transport equations.

These electrons are accelerated to the detection region by the drift electric field. The macroscopic drift behavior of these electrons can be described by the mean drift velocity $v_{||}$ and magnetic deflection angle α. Using classical drift theory [10] the microscopic interactions which lead to these macroscopic quantities can be examined. For simplicity, the mean velocity from the velocity distribution will be used and diffusion ($\sim 70\mu$m) will be neglected.

2.1 Classical drift theory

Consider an electron moving through a gas mixture under the influence of perpendicular electric and magnetic fields,

$$\boldsymbol{E} = (E_x, 0, 0), \tag{2.1a}$$

$$\boldsymbol{B} = (0, 0, B_z). \tag{2.1b}$$

The electron is acted upon by these fields as described by the Lorentz force law,

$$m\frac{d\boldsymbol{v}}{dt} = e\boldsymbol{E} + e(\boldsymbol{v} \times \boldsymbol{B}) \tag{2.2}$$

where m is the electron mass, $\boldsymbol{v}$ is the electron velocity, and e is the electron charge. Plugging in the non-zero vector components from Eqs. 2.1, the following coupled components of the acceleration vector are found:

$$\dot{v}_x = \varepsilon + \omega v_y \tag{2.3a}$$

$$\dot{v}_y = -\omega v_x \tag{2.3b}$$

$$\dot{v}_z = 0 \tag{2.3c}$$

where $\varepsilon = (e/m)E_x$ and $\omega = (e/m)B_z$. These equations can be solved by substitution and the constants of integration can be found using the initial conditions that $\boldsymbol{v} = 0$ when $t = 0$. These solved equations describe the velocity of the electron between collisions with molecules in the gas:

$$v_x(t) = \frac{\varepsilon}{\omega}\sin\omega t \tag{2.4a}$$

$$v_y(t) = \frac{\varepsilon}{\omega}(\cos\omega t - 1) \tag{2.4b}$$

$$v_z(t) = 0. \tag{2.4c}$$

These microscopic velocities can be folded with the time distribution of collisions to give macroscopic average velocities for the electron. Therefore, the expression for the distribution of times between collisions must be derived.

The average time between collisions[1] τ is found from the average momentum gained by the electron between collisions. This is equal to τ times the force on the electron eE. This can be rearranged to give:

$$\tau = \frac{mu}{eE} \tag{2.5}$$

where u is the microscopic velocity of the electron.

The probability distribution for a collision between times t and $t + dt$ after the previous collision is given by

$$f(t)dt = \frac{1}{\tau} e^{-t/\tau} dt. \tag{2.6}$$

The following integral can be carried out on the three velocity components:

$$< v_i >= \int_0^\infty f(t) v_i(t) dt, \tag{2.7}$$

yielding

$$< v_x >= \frac{\varepsilon\tau}{1+\omega^2\tau^2} \tag{2.8a}$$

$$< v_y >= -\frac{\varepsilon\omega\tau^2}{1+\omega^2\tau^2} \tag{2.8b}$$

$$< v_z >= 0. \tag{2.8c}$$

Note that $\omega\tau$ can be of order 1 in present detectors.

[1] This time is energy dependent and is inversely proportional to the cross-section σ.

2.1.1 Drift velocity

By adding the velocity components in Eqs. 2.8 in quadrature, the magnitude of the drift velocity v, is found to be

$$v = \frac{\varepsilon\tau}{\sqrt{1+\omega^2\tau^2}}. \tag{2.9}$$

The quantity measured is the drift velocity of the electron parallel to the electric field $v_{||}$, which is given by Eq. 2.8a.

2.1.2 Magnetic deflection angle

The magnetic deflection angle α is the angle between the drift velocity and the electric field vectors. The tangent of this angle is given by the ratio of Eqs. 2.8b and 2.8a:

$$\tan\alpha = \omega\tau. \tag{2.10}$$

By substituting for ω and τ a simple expression for the magnetic deflection angle is arrived at:

$$\tan\alpha = \frac{e}{m}\cdot\frac{mu}{eE} = u\frac{B}{E}, \tag{2.11}$$

which agrees with the Lorentz force law.

2.2 Scaling laws

In this section, simple relations are established which allow easy interpolation of data under different conditions.

2.2.1 Scaling for magnetic field

The mean drift velocity is the component of the total electron velocity parallel with the electric field (Eq. 2.8a)

$$v_{||} = v_{total}\cos\alpha. \tag{2.12}$$

Low magnetic fields (< 1 Tesla) do not have a large effect on the total drift velocity. Thus, given $v_{||}(E, B = 0)$ and $\alpha(E, B \neq 0)$, $v_{||}(E_{mod}, B \neq 0)$ can be predicted. E_{mod} is the electric field parallel to the total velocity:

$$E_{mod} = E \cos \alpha. \tag{2.13}$$

This can greatly reduce the amount of data needed to describe electron drift[2].

Now consider Eq. 2.11. The $\tan \alpha$ is proportional to the magnetic field strength. Therefore, if the magnet field strength is doubled, the tangent of the angle is also doubled. The following relation describes this:

$$\frac{\tan \alpha_1}{B_1} = \frac{\tan \alpha_2}{B_2}. \tag{2.14}$$

This means that given a velocity and an angle at a non-zero magnetic field, *all* velocities and angles can be calculated at E_{mod}.

2.2.2 Scaling for pressure

Consider an electron in a gas mixture at 1 bar. Under the application of an electric field, the electron will be accelerated until it collides with a gas molecule. The average distance between collisions is called the mean free path[3] λ. This distance is directly related to the number density of gas molecules which in turn is directly related to the pressure of the gas at constant temperature[4]. Therefore, if the pressure of the gas is raised to 3 bar, λ will by divided by three. For the electron to drift at the same energy, the electric field must be increased by a factor three. Thus, given v_{total} and E at P_o, v_{total} is known for $E \to E \cdot \frac{P}{P_o}$, where $\frac{P}{P_o}$ is the ratio of the pressures[5].

The angles can also be scaled for pressure according to the same reasoning. At a magnetic field B, the amount of deflection from the bent trajectory of the electron gets

[2] This is described in more detail in [11] and references therein.

[3] The mean free path is on the order of 10^{-5} m at 1 bar and is related to τ by σ.

[4] Assuming ideal gas laws.

[5] Scaling for temperature can be done, but by using the equation of state for an ideal gas, $PV = Nk_BT$, the temperature change can be incorporated into the pressure change.

smaller with smaller λ. By increasing the magnetic field, the deflection is increased, thus achieving the same trajectory in a higher pressure. Thus increases in pressure have the opposite effect of increases in magnetic field. Using the example from above, if the pressure is increased by a factor $\frac{P}{P_o}$, the effective magnetic field is $B/\frac{P}{P_o}$.

2.3 Space-time relation for a cylindrical geometry

The goal of this section is to derive an expression for the time an electron takes to drift to the wire in a drift tube. First, consider a small radial element, $d\boldsymbol{r}$, located a distance $\boldsymbol{r}$ from the axis of the tube. The electric field as a function of radius is

$$\boldsymbol{E}(\boldsymbol{r}) = \frac{\lambda_Q}{2\pi\epsilon_o r}\hat{\boldsymbol{r}} \tag{2.15}$$

where λ_Q is the charge density on the wire. The drift velocity of electrons at $\boldsymbol{E}(\boldsymbol{r})$ can be measured, yielding the velocity as a function of radius. Dividing the differential distance by the velocity gives the differential time:

$$\frac{d\boldsymbol{r}}{\boldsymbol{v}(\boldsymbol{r})} = dt. \tag{2.16}$$

Integrating this expression yields

$$t' = \int_{r'}^{r_{wire}} \frac{d\boldsymbol{r}}{\boldsymbol{v}(\boldsymbol{r})}, \tag{2.17}$$

where t' is the time the electron takes to drift from the tube radius r', to the wire radius r_{wire}.

The drift velocity data can be changed from a function of electric field to a function of radius using Eq. 2.15. This set of points can then be fit to a high order polynomial, so that the integration in Eq. 2.17 can be performed giving radius as a function of time $\boldsymbol{r}(t)$.

The space resolution which can be achieved by a drift tube is strongly dependent on the linearity of the space-time curve. From the description above, it is clear that a constant $\boldsymbol{v}(\boldsymbol{E})$ leads to a linear space-time curve. This means that the electron velocity is independent of electric field, implying that the electron velocity will not be affected by irregularities in the electric field caused by space charge effects, especially in the amplification region near the wire. In practice there is no gas mixture with a constant $\boldsymbol{v}(\boldsymbol{E})$ over the needed range of electric field. However, some gas mixtures come close to having a constant velocity except in the region close to the wire ($r' < 1$ mm).

Chapter 3

Experimental setup[1]

3.1 Gas system

Gases are either bought pre-mixed or mixed into evacuated bottles by adding partial pressures which are monitored by a pressure transducer. The error on this method is estimated to be less than 1/2%. Bottles of mixed gas stand overnight to ensure proper mixing of the gases. The drift chamber is evacuated and then connected to the gas system. When measurements are taken at atmospheric pressure, the gas flow is regulated before the chamber so that the pressure drop from the flow meter to atmosphere is minimal[2]. For data taken at overpressure, this initial flow meter is bypassed and the meter on the outflow from the chamber is set low. The pressure at the chamber is set from the bottle regulator.

3.2 Multi-wire proportional chamber

The main apparatus consists of a multi-wire proportional chamber (Fig. 3-1) placed in the former cyclotron magnet (Fig. 3-2) in building 44 at MIT. The drift region of the chamber is well approximated by a parallel plate capacitor which generates an electric field. The high voltage cathode plate is copper clad G10, a material used

[1]The basic design is given in [12]. An overview and changes are given here.
[2]The drop has been measured with a manometer to be less than 1 mbar.

for its mechanical strength and insulating properties, and the anode ground is 0.5 mm copper mesh, which is semi-transparent to the drifting electrons. The chamber is situated so that the electric field is perpendicular to the vertical magnetic field. For field homogeneity, wires connected to voltage dividers are wrapped around the chamber and used to step down the voltage between the cathode and anode. Behind the mesh is a proportional chamber which amplifies and detects the drifting electrons. The influence of the amplification process on data is eliminated by taking differential measurements.

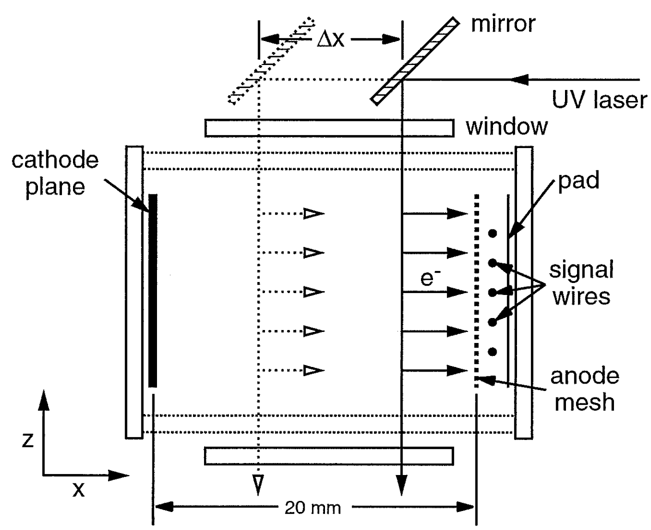

(a)

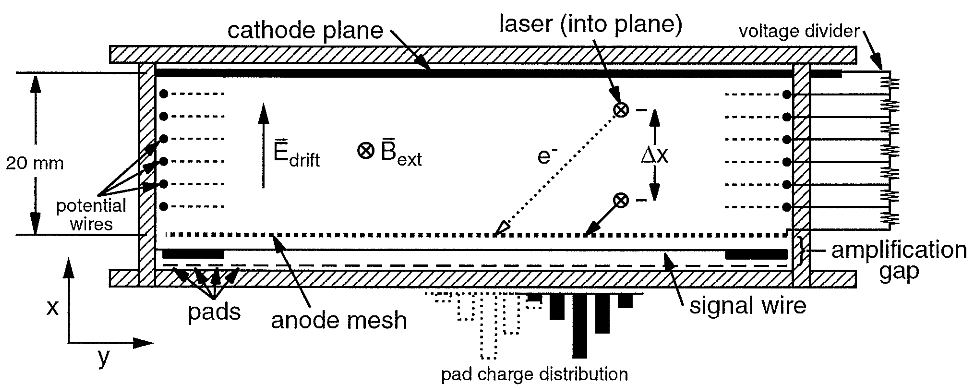

(b)

Figure 3-1: Schematic representation of the chamber used to measure drift velocity and magnetic deflection angle: (a) side view shows UV laser beam displacement and (b) top view shows pad distribution for magnetic deflection angle measurement [11].

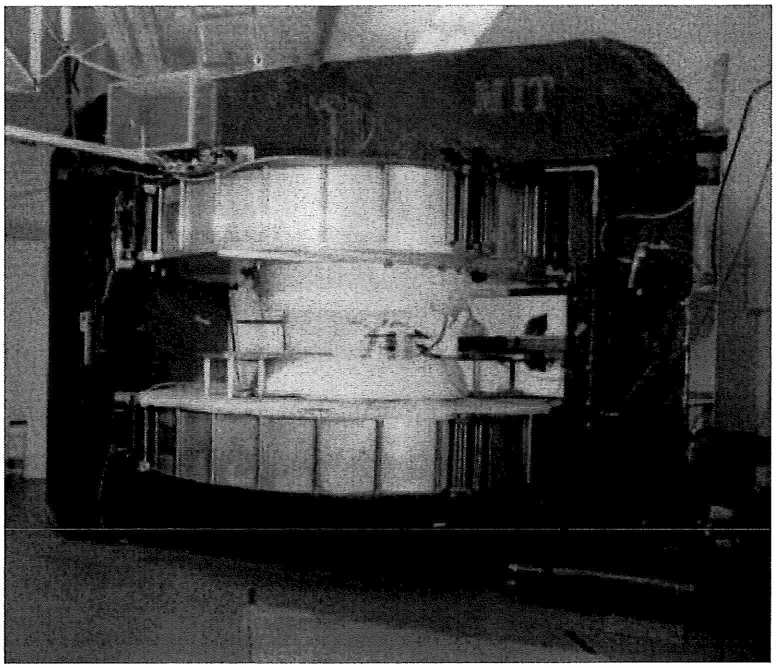

Figure 3-2: MIT cyclotron electromagnet in building 44.

3.3 Laser and optics setup

A pulse from a 337 nm N_2 laser [13] simulates the gas ionization of a high energy particle in the chamber. The laser is run through a series of UV lenses, which focus the beam inside the chamber. A 1000 μm aperture is used to eliminate stray light from the beam. This stray light reflects from the metal around the aperture into a photodiode, which triggers the electronics. The laser impinges the magnet volume horizontally and is reflected 90° down into the chamber by a UV Enhanced aluminum mirror. The mirror is fixed to a one-dimensional micrometer with its degree of freedom along the axis of the laser. This micrometer is used to change the path of the laser between the cathode plate and the anode mesh.

3.4 Magnet

The cyclotron electromagnet (1938) generates a magnetic field which is 99% homogeneous over the area of the drift chamber. A maximum magnetic field of about 1.4 T is achievable with iron slabs bolted to the top pole-face which concentrate the magnetic field into the volume in which the chamber lies.

3.5 Measured quantities

3.5.1 Drift velocity measurement, $B = 0$

The electrons from the gas ionization initially have a random distribution of velocities and are accelerated towards the mesh by the electric field. After passing through the mesh, the electrons are collected on five high voltage signal wires which are horizontally situated perpendicular to the electric field. The wires are capacitively coupled to amplifiers which make the resulting signal large enough to trigger the electronics. The time taken by the electrons to drift across the electric field is measured by time-to-digital converters (TDCs) [14] which measure the time between a start pulse from the photodiode signal and a stop pulse from the output of the signal wire amplifiers.

Drift times at two mirror positions can be measured and the time difference Δt is equal to the time taken by the electrons to drift the distance between the two mirror positions[3] Δx ($\sim 1\,\mathrm{cm}$). The mean drift velocity v_{drift} is defined as

$$v_{\mathrm{drift}} = \frac{\Delta x}{\Delta t}. \tag{3.1}$$

One hundred laser events are averaged at each mirror position.

3.5.2 Drift velocity measurement, $B \neq 0$

When a magnetic field is present, the direction of the acceleration of the electron in a mean free path is changed. Instead of being accelerated in a straight line towards the mesh, the electron travels with a cycloidal motion which is interrupted by its frequent collisions with the gas atoms of molecules. These small pieces of cycloidal motion add up to a straight macroscopic drift path at an angle to the electric field.

[3] This is valid as long as the drift distance is much greater than the mean free path of the electrons in the gas.

In the case of $B \neq 0$, the component of the drift velocity *parallel* to the electric field $v_{||}$ is measured.

3.5.3 Magnetic deflection measurement

Twenty-four segmented pads vertically situated behind the signal wires are used to measure the angle between the total drift velocity and the electric field. Voltages are induced on these pads by the signals collected on the wires. These voltage signals are amplified and fed into analog-to-digital converters (ADCs) [15] which integrate over an external time gate. A weighted average of the integrated charge values gives the "center pad" of the spatial electron distribution, which describes the position in the chamber where the signal hits the wire. Using simple trigonometry and the averages from the differential measurements, the magnetic deflection angle can be calculated.

3.6 Hardware and software

The outputs from the TDCs and ADCs are read by a CAMAC crate and transmitted to a PC via GPIB. LabView software was written for data acquisition and analysis. Upgraded features include easy setting of hardware parameters (number of TDC or ADC channels, chamber geometry, etc.) and a graphical user interface.

Chapter 4

Data and results for scaling laws

Data sets of electron mean drift velocity and magnetic deflection angle were taken in P10 gas[1] at atmospheric pressure and 3 bar (Figs. 4-1) to compare the magnetic field and pressure scaling described in Sec. 2.2. Errors on the drift velocity and angles are estimated to be 1% and 0.5°.

4.1 Data scaling for magnetic field

4.1.1 Velocity scaling

By applying Eq. 2.12 to each velocity point, a total velocity is found which is independent of α after the electric field is modified. The results of this analysis are shown in Fig. 4-2. To a good approximation, Eq. 2.12 describes the scaling well for $E > 0.1$ kV/cm and $B < 1$ T.

4.1.2 Angle scaling

In Fig. 4-3, the result of scaling the magnetic deflection angle for magnetic field is presented. The tangents of the various angles were divided by the magnetic field. The arctangents were then taken to return the quantities to angular units. Eq. 2.14 well describes the data.

[1]A mixture of Ar:CH_4 (90:10)%.

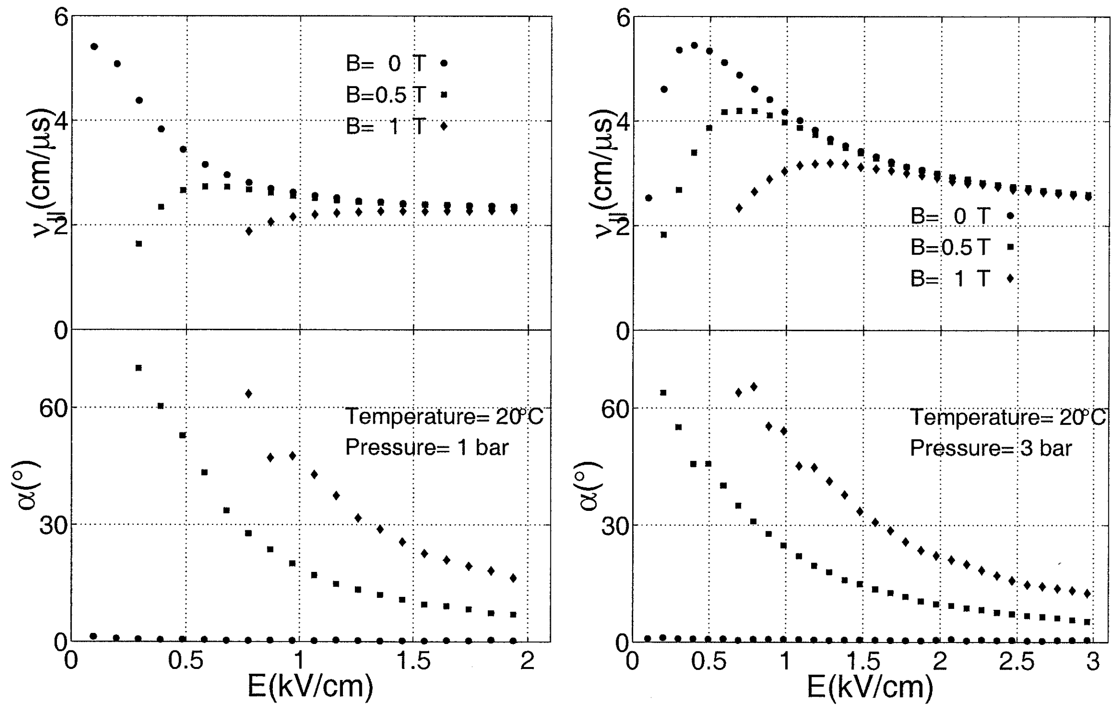

(a) 1 bar

(b) 3 bar

Figure 4-1: $v_{||}$ and α data taken at different pressures in P10.

4.2 Data scaling for pressure

4.2.1 Velocity scaling

The data from Figs. 4-1 were used to demonstrate pressure scaling. The electric fields were divided by the pressure in bar for velocity data taken without an external magnetic field. These scaled data are shown in Fig. 4-4.

4.2.2 Angle scaling

The effect on angles of increasing pressure is the opposite of increasing magnetic field. Thus the tangents of the angles were multiplied by the pressure before being returned to angular units. The scaled data are shown in Fig. 4-5.

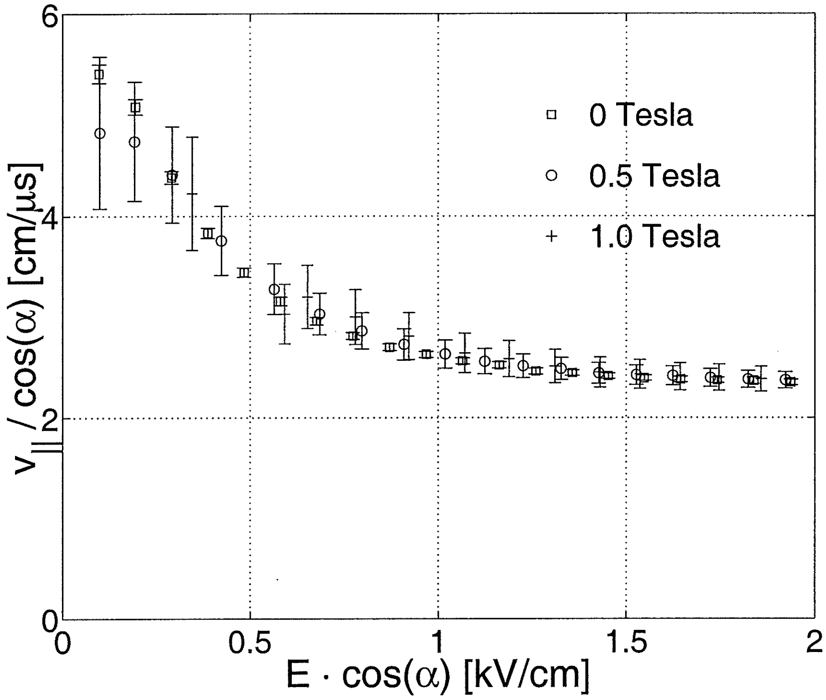

Figure 4-2: Velocity scaling for different magnetic fields.

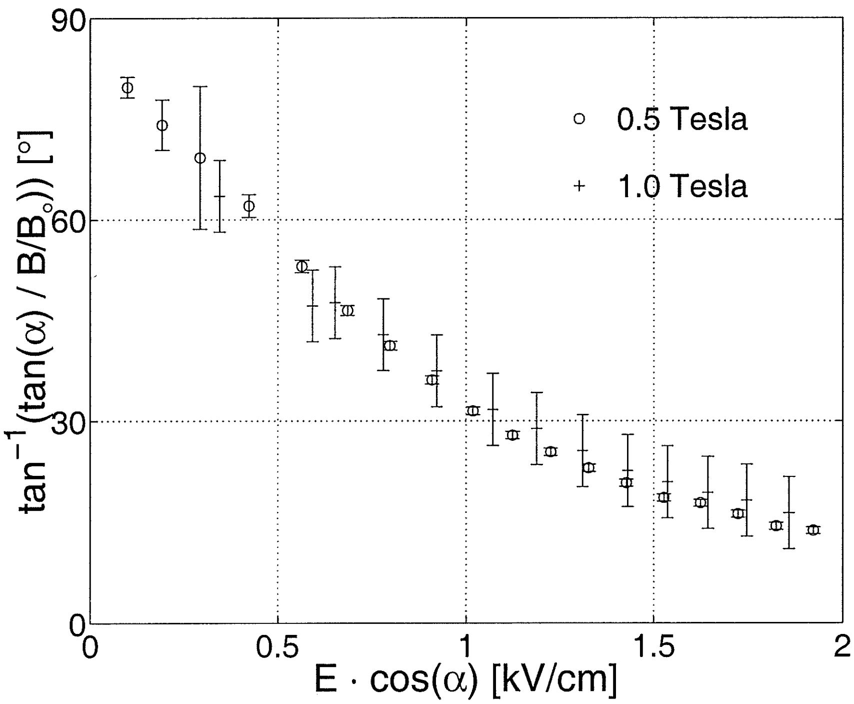

Figure 4-3: Angle scaling for different magnetic fields. B_o is 1 Tesla.

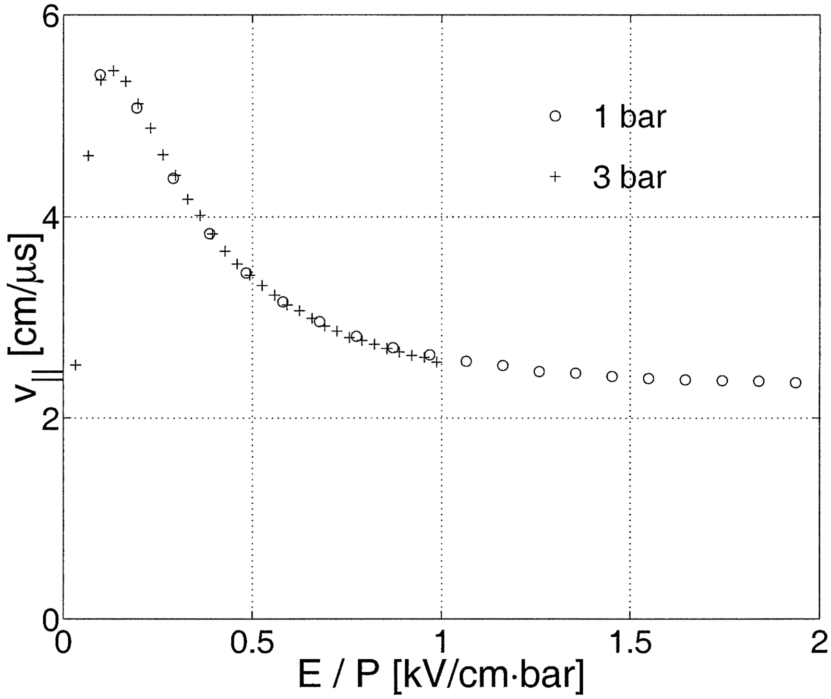

Figure 4-4: Velocity scaling for different pressures.

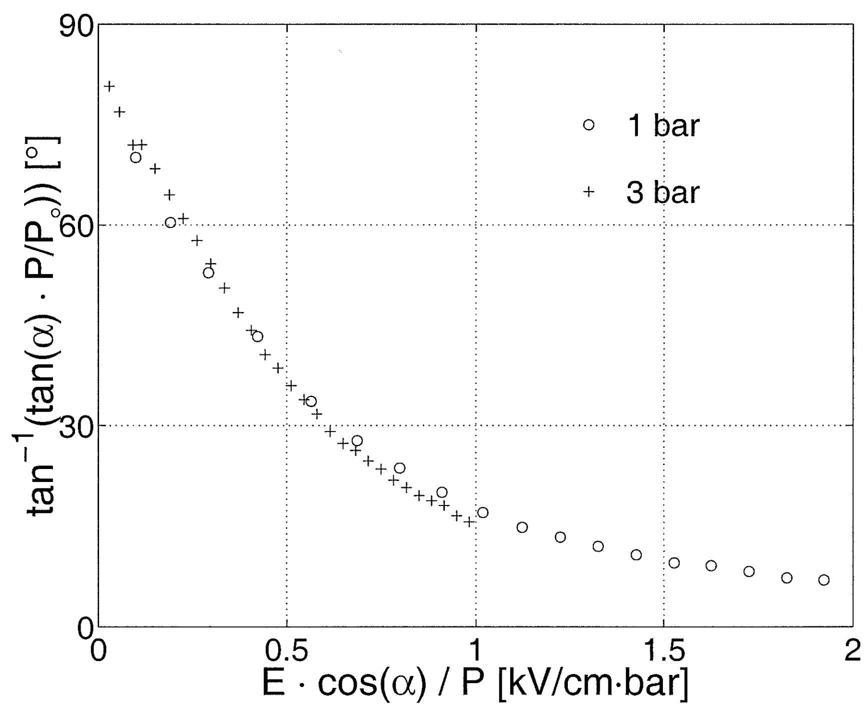

Figure 4-5: Angle scaling for different pressures. $P_\circ$ is 1 bar.

Chapter 5

Results for a better space-time relation

5.1 Space-time relation

A drift tube chamber measures times which are converted into coordinates by its space-time relation. To predict these relations, mean drift velocities and magnetic deflection angles in various gas mixtures were measured. The ATLAS collaboration originally proposed to use Ar:CH_4:N_2 (91:5:4)% [1], which has a highly linear space-time relation as shown in Fig. 1-3. Following the method described in Sec. 2.3, a numerical integration of Eq. 2.17 was performed, yielding a radius versus time plot which agrees with ATLAS results (compare Fig. 5-1(a) with Fig. 1-3).

Many mixtures were studied in both experiment and in Monte Carlo simulations using Magboltz[1] [16]. Two mixtures which looked interesting in simulation were experimentally measured for verification: Ar:N_2:CO_2 (94:2:4)% and (92:6:2)%. The originally proposed ATLAS MDT drift gas mixture, Ar:CH_4:N_2 (91:5:4)%, was chosen because it has a drift velocity which is almost independent of electric field, resulting in a linear space-time curve. However, further analysis showed that gases with CH_4 or other organic admixtures accelerated ageing processes [2] [3] [4]. By default, Ar:CO_2

[1]Magboltz performs a Monte Carlo simulation of electron transport in gas mixtures in electric and magnetic fields.

(93:7)% is being used as a replacement gas [4]. This gas is slower and more non-linear than the originally proposed mixture (compare Fig. 5-1(a) and Fig. 5-1(b)) making the dead time of the drift tube much longer than 500 ns and the error due to electric field and pressure uncertainty larger. Positive features of this gas are its lower magnetic deflection angles and resistance to ageing [4].

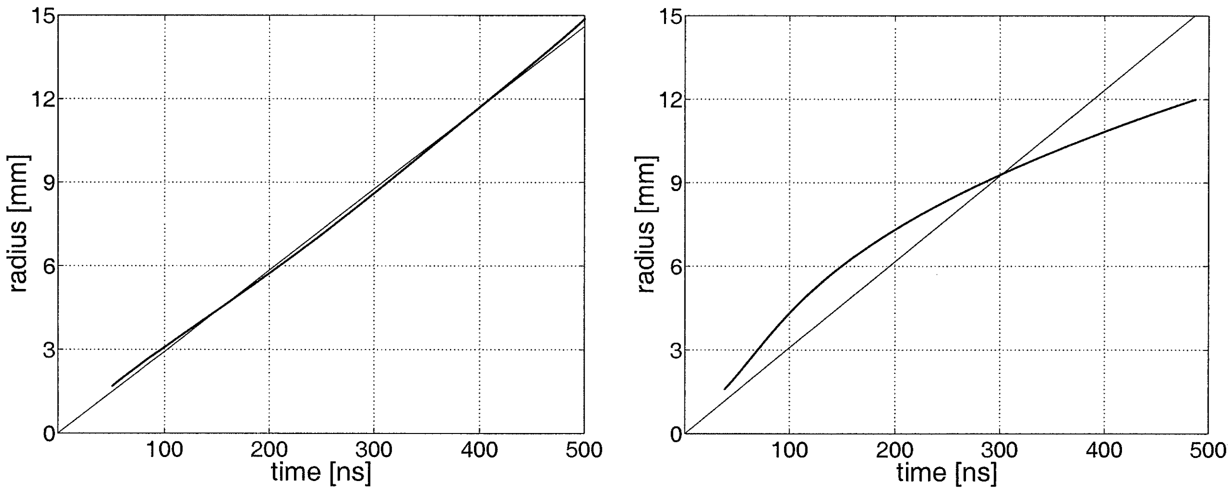

(a) $Ar:CH_4:N_2$ (91:5:4)%

(b) $Ar:C0_2$ (93:7)%

Figure 5-1: Space-time curves from analysis of $v_{||}$ data at $B = 0$. The lighter line is a maximum likelihood linear fit constrained to go through the origin.

5.2 Discussion of ingredients

The improvement of performance over the $Ar:CO_2$ (93:7)% mixture is based on the electron-gas interaction cross-sections of admixture gases (Figs. 5-2). Due to quantum mechanical effects, these cross-sections are a function of energy. For example, the cross-section of Ar has a minimum at about 0.23 eV, meaning that when electrons have this energy, they interact less with the Ar atoms. This explains the maximum in drift velocity of gas mixtures containing Ar (Figs. 4-1). CO_2 has a large inelastic cross-section at low energy which tends to keep the mean electron energy low and around that of the Ar cross-section minimum [8]. This strongly increases non-linearity, but the smaller average time between collisions leads to smaller angles (Eq. 2.10).

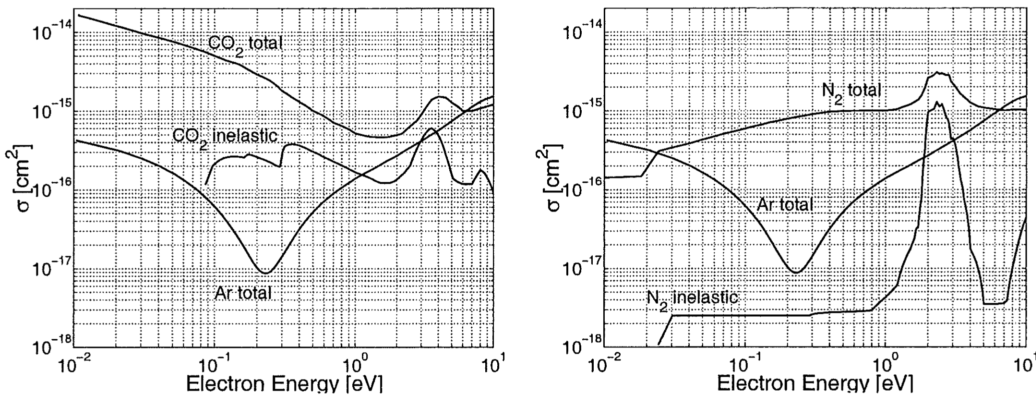

(a) Ar vs. CO_2 (b) Ar vs. N_2

Figure 5-2: Energy dependent electron-gas interaction cross-sections [16].

5.3 Results from new mixtures

In order to obtain a more constant electron velocity at low electric field, the amount of CO_2 was reduced. The addition of N_2 to an Ar:CO_2 mixture was advantageous at higher electric fields. N_2 has a large elastic cross-section which helps to diminish the effect of the minimum in the Ar cross-section. Thus, the addition of N_2 should flatten the drift velocity curve and straighten the space-time relation. The negative effect is an increase in deflection angle. The data in Figs. 5-3 show the effects described above. The velocities in Figs. 5-3(b) and 5-3(c) lead to much better space-time curves as seen in Figs. 5-4 and the magnetic deflection angles are not much higher than the presently used mixture.

5.4 Discussion of accuracy

To see the benefits of a linear drift gas, a simple model consisting of a two-layer set of drift tubes is considered (Fig. 5-5(a)). Muon track 1 is the actual path of the muon, but due to non-linearities in the space-time relation, this track will be incorrectly reconstructed. At 60° from vertical, muon track 2 is also affected by these non-linearities. Fig. 5-5(b) shows the systematic errors when three-layers of drift tubes are used. The third layer helps to pull the reconstructed muon track 1 back

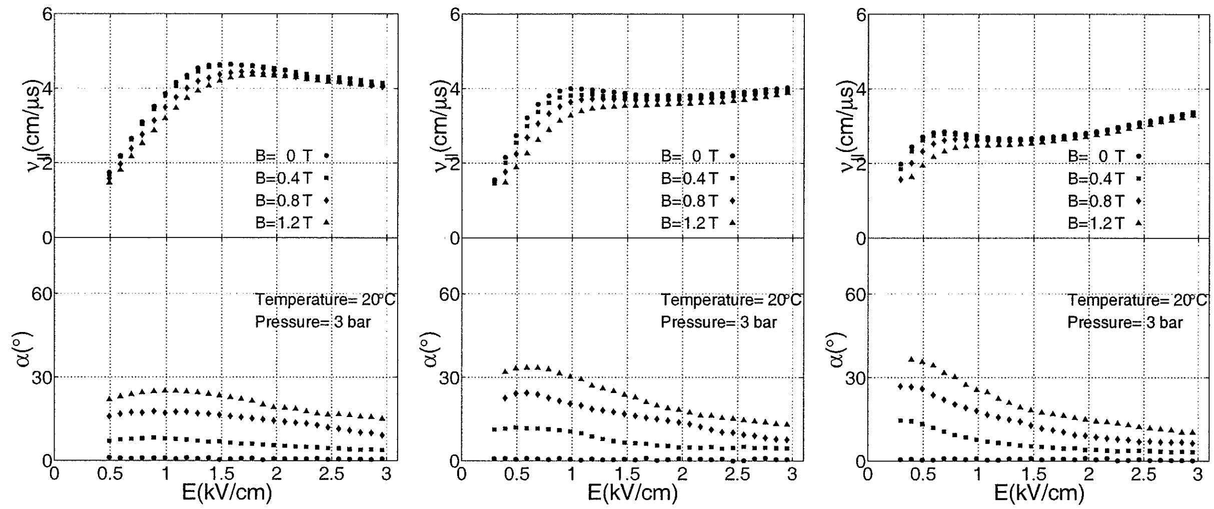

(a) Ar:CO_2 (93:7)% (b) Ar:N_2:CO_2 (94:2:4)% (c) Ar:N_2:CO_2 (92:6:2)%

Figure 5-3: $v_{||}$ and α data taken in mixtures of Ar, N_2, and CO_2.

to vertical, but the reconstructed muon track 2 continues to suffer from the wrongly predicted radii.

Using the space-time curves from Figs. 5-1(b) and 5-4, horizontal deviations in the muon track reconstruction were calculated for muons impinging vertically and at 60° from vertical. These errors are shown in Figs. 5-6. It is clear that the reconstruction error in a gas is strongly related to the linearity of its space-time relation.

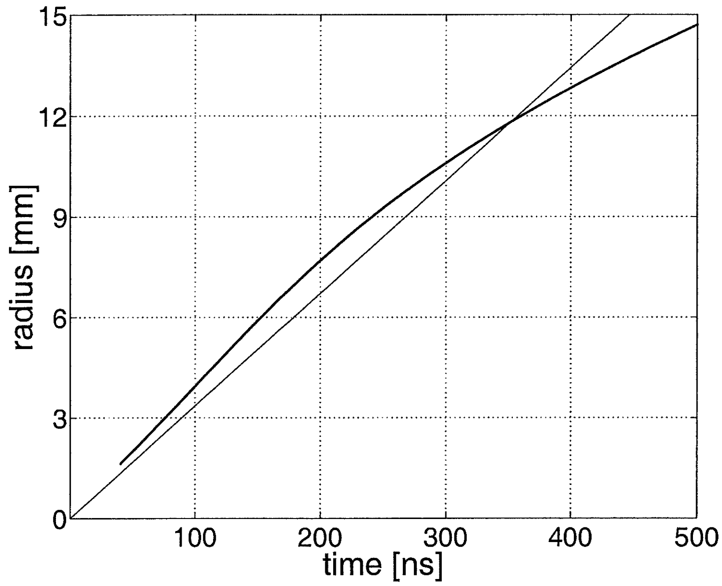

(a) Ar:N_2:CO_2 (94:2:4)%

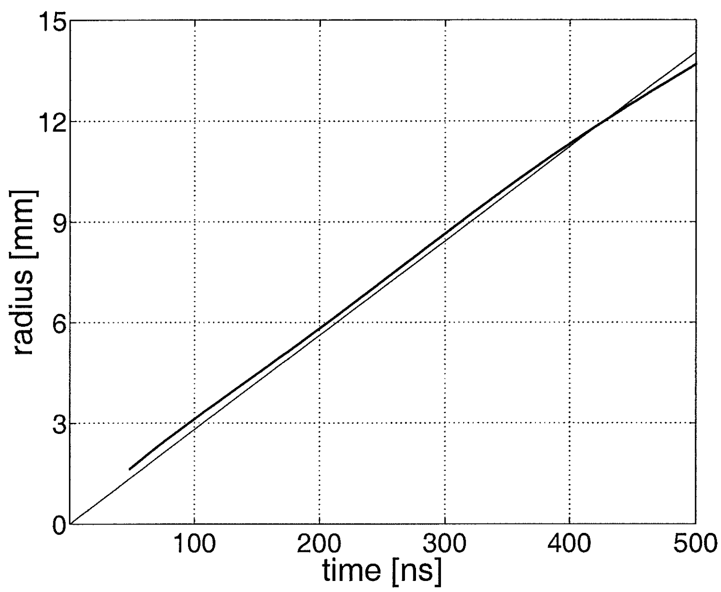

(b) Ar:N_2:CO_2 (92:6:2)%

Figure 5-4: Space-time curves and linear fits for mixtures of Ar, N_2, and CO_2.

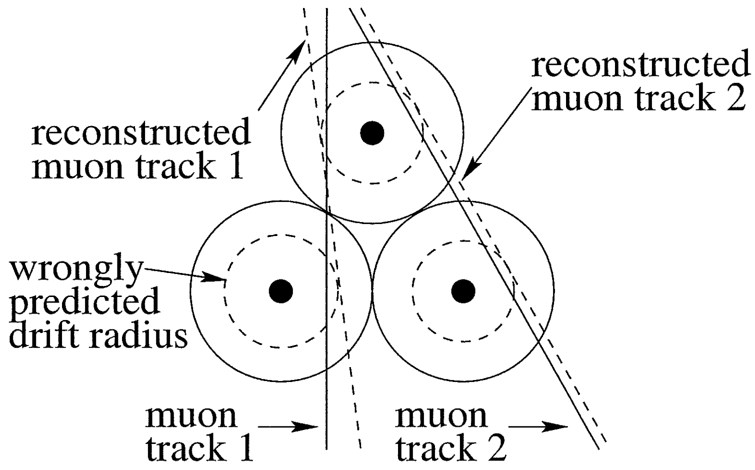

(a) Two layers

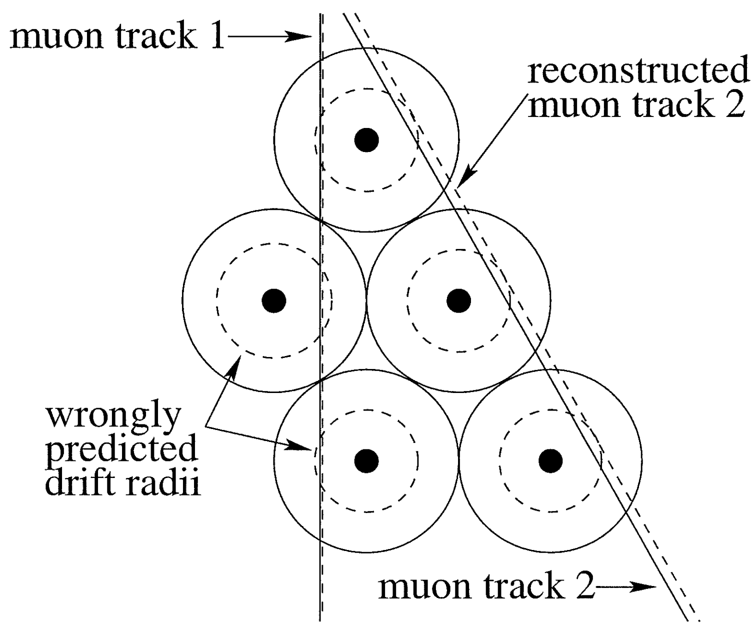

(b) Three layers

Figure 5-5: Schematic describing resolution degradation due to non-linearities in the space-time curve.

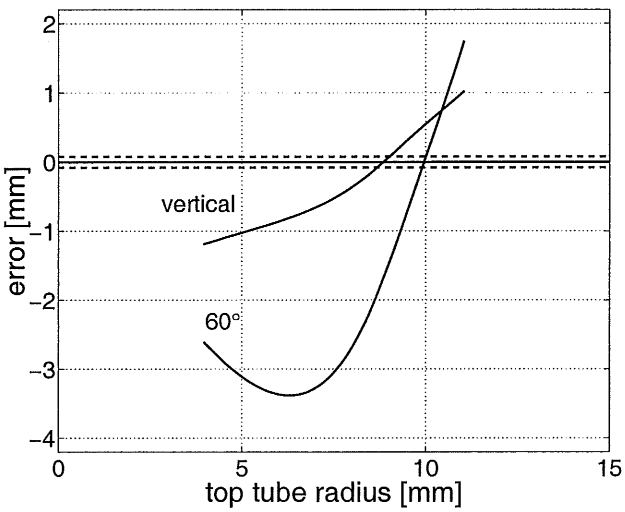

(a) Ar:CO_2 (93:7)%

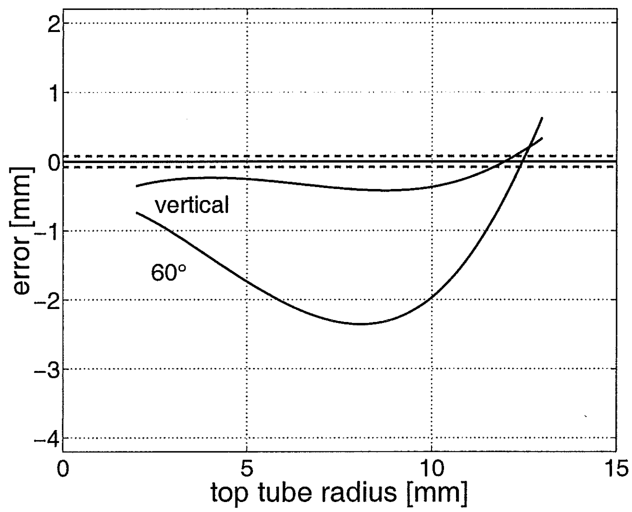

(b) Ar:N_2:CO_2 (94:2:4)%

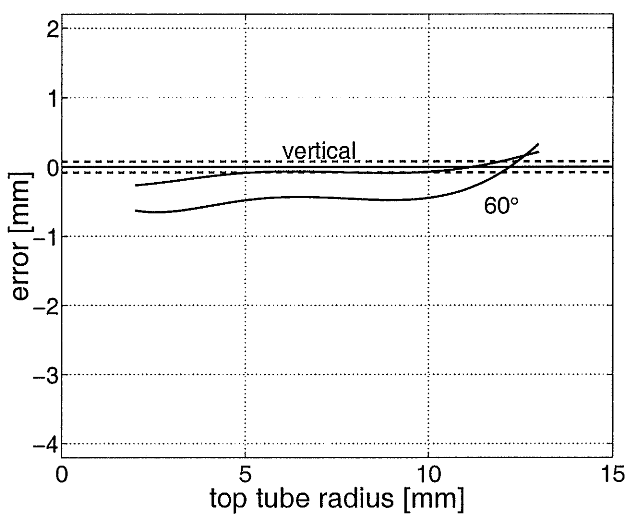

(c) Ar:N_2:CO_2 (92:6:2)%

Figure 5-6: Reconstruction errors in mixtures of Ar, N_2, and CO_2. The dashed lines represent the ATLAS resolution goal of 80 μm.

Chapter 6

Conclusions

This thesis presents new data on detector gases. It was shown that simple relations can be used to scale mean drift velocity and magnetic deflection angle data for magnetic field and pressure. Applying data to a cylindrical geometry allowed a search for a gas with a nearly linear space-time relation.

With knowledge of gas additions, definite improvements over the present mixture of $Ar:CO_2$ (93:7)% in the ATLAS MDT system were found. $Ar:N_2:CO_2$ (94:2:4)% gives roughly a factor three improvement and $Ar:N_2:CO_2$ (92:6:2)% has an order of magnitude smaller corrections and may provide a chance to improve accuracy in the 100 million dollar detector.

Bibliography

[1] Atlas muon spectrometer: Technical design report. CERN-LHCC-97-22.

[2] G. Herten. University of Freiburg, private communication, 1998.

[3] M. Kollefrath et al. Ageing studies for the ATLAS-monitored drift tubes. *Nucl. Instrum. Meth.*, A419:351, 1998.

[4] M. Aleksa and W. Riegler. Non-linear MDT drift gases like Ar/CO_2. ATL-MUON-98-268.

[5] ATLAS public homepage. `http:\\www.cern.ch\atlas\`.

[6] S. Ahlen. Boston University, private communication, 2000.

[7] U. J. Becker, S. C. Nahn, J. P. Rodin, and B. R. Smith. Effect of N-2 contamination on drift chambers in magnetic fields. *Nucl. Instrum. Meth.*, A351:583–584, 1994.

[8] E. Fortunato, U. Becker, and R. Dinner. Understanding the impact of additives with large inelastic cross-sections on drift chamber performance. *Nucl. Instrum. Meth.*, A421:278, 1999.

[9] D. E. Groom. Passage of particles through matter: in Review of Particle Physics (RPP 1998). *Eur. Phys. J.*, C3:144–151, 1998.

[10] W. Blum and L. Rolandi. Particle detection with drift chambers. Berlin, Germany: Springer (1993) 348 p.

[11] U. Becker et al. Consistent measurements comparing the drift features of noble gas mixtures. *Nucl. Instrum. Meth.*, A421:54, 1999.

[12] U. Becker et al. Calibration setup for drift chamber gases. *Nucl. Instrum. Meth.*, A306:194, 1991.

[13] VSL-337ND Nitrogen Laser. Laser Science, Inc.

[14] LRS 2229 TDC. Lecroy Research Systems.

[15] LRS 2249W ADC. Lecroy Research Systems.

[16] S. F. Biagi. A multiterm Boltzmann analysis of drift velocity, diffusion, gain and magnetic field effects in argon methane water vapor mixtures. *Nucl. Instrum. Meth.*, A283:716, 1989. and University of Liverpool, private communication.